Modern Electronic Materials 3 (2017) 131–141

Contents lists available at ScienceDirect

Modern Electronic Materials

journal homepage: www.elsevier.com/locate/moem

The use of AES and EELS for complex analysis of two-dimensional coatings and their growth process

Nikolay I. Plusnin

Department of Physics of Nanostructures, Institute of Automation and Control Processes of the Far Eastern Branch of the Russian Academy of Sciences, 5 Radio Str., Vladivostok 690041, Russia

ARTICLE INFO

Keywords:
PVD
AES
EELS
Two-dimensional coatings
Wetting nanophase layer
Sub-nanometer thickness
Quantitative Auger analysis
Plasmon satellite of Auger peak
Localization of places of adsorption
EELS depth profiling
Metal
Silicide
Silicon

ABSTRACT

Additional possibilities for complex analysis of two-dimensional coatings (thickness < 1 nm or < 10 ML) grown by physical vapor deposition (PVD) on a single-crystal silicon substrate under two deposition regimes have been revealed: 1) low-temperature (at a low beam temperature) and 2) high-temperature (at an elevated temperature of the beam), respectively. Coatings, including those in the form of pure metal and a silicide mixture, and their interface with the substrate have been analyzed by Auger electron spectroscopy (AES) and characteristic electron energy loss spectroscopy (EELS). A technology of the deposition from a ribboned source has been developed to ensure both deposition regimes. The conventional uses of AES are limited to the characterization of elemental composition, electron energy structure and coating thickness. For EELS, the conventional uses are the determination of phase types (valence electron density) and phase formation stages. The simultaneous use of the two methods and the choice of equal (and minimal) probing depths, ~ 2.5 nm (primary electron energy 300 eV), provided new possibilities for studying subnanometric two-dimensional coatings, in particular, for comparison of coating composition and density. The chosen probing depth also made it possible to characterize the interface between the coating and the substrate. At the same time, the use of similar probing depths made allowed using the thickness of the coating obtained from AES data for analyzing EELS data. In addition, other possibilities have been considered, i.e., the use of the following dependences: a) the energy of the plasmon satellite of the Auger peak *vs* the thickness of the coating for analyzing changes in the electron density in the near-interface layer of silicon; b) the attenuation of the Auger signal generated by marker atoms at the interface between the coating and the substrate for localizing the adsorption sites of the deposited atoms; c) the intensity and energy of the loss peaks in the EELS as a function of the primary electron energy for depth profiling of coating compositions. The use of two depth attenuation functions for two probing depths has enabled a quantitative Auger analysis of binary coatings. These advantages have provided the possibility of a more complete characterization of two-dimensional coatings and their interfaces with substrates, as well as the coating formation processes. In particular, it has for the first time become possible to identify the wetting nanophase layer of metals on silicon substrates, to investigate the process of its formation and to show how its composition depends on vapor-phase physical deposition modes.

Introduction

The development of new two-dimensional materials which may find application in electronics [1], e.g. monoatomic [2] and thicker (multiatomic [3] or wetting [4]) metallic coatings on silicon substrates, enabled new phase structure and chemical state characterization methods. Of special interest among these methods are Auger electron spectroscopy (AES) and characteristic electron energy loss spectroscopy (EELS). These two methods allow characterization of coatings in vacuum during physical vapor deposition (PVD).

Indeed, AES and EELS find broad application for the *in situ* characterization of element ratios in coatings [5], as well as their chemical [6] and phase [7] states.

The conventional use of AES is the composition analysis of bulk specimens [8–10], including destructive ion beam etching composition depth profiling methods [11]. In the latter case the Auger primary electron energy is high (2500+ eV). This provides for better beam focusing which is of special importance for scanning Auger spectroscopy and minimizing the effect of the surface on the results of analysis for the specimen bulk. Quantitative Auger characterization provided tabulated

Peer review under responsibility of the National University of Science and Technology MISiS.
E-mail address: plusnin@iacp.dvo.ru.

https://doi.org/10.1016/j.moem.2017.12.001
Received 11 October 2017; Accepted 27 November 2017

data for elemental sensitivity coefficients of various bulk materials [12].

Regarding the conventional use of EELS, this is primarily the energy selective imaging in electron microscopy [13]. The method is used for the phase (valence electron losses) or elemental (deep level ionization losses) mapping of bulk specimen composition by electron energy filtering in the characteristic loss region. Another important application of the method is the quantitative elemental composition characterization by deep level ionization [13]. Since recently valence electron EELS has been used in electron microscopy for indirect phase hardness mapping [14]. Also known is EELS use for composition characterization of binary systems by elastic peak intensity [4,15] or from the integral valence electron energy loss spectrum [16].

Before the 1990s the AES and EELS methods were used for the phase structure analysis of surface and the surface phases [17]. However, that use only replicated their conventional applications. Later the interest to the methods expired due to the development of simple methods of scanning probe microscopy / spectroscopy which are more information valuable and sensitive to surfaces and monolayers [18].

Many works and overviews published before the mid-1990s dealt with EELS and especially AES analysis. However, there have been noticeably fewer AES overviews [19,20], the same being in the EELS literature, except for high resolution EELS in vibration peak analysis at energies of up to hundreds meV. There are only an overview of EELS in electron microscopy [21] and an EELS map of surface phases [22], but neither of these works dealt with two-dimensional coating analysis with these methods.

However, AES and EELS are indispensable in specific areas. One of them is subnanometer coating thickness analysis (two-dimensional coatings). The other application relates to coatings which may be not single crystalline and coatings that form under nonequilibrium growth conditions. Examples are PVD metallic coatings on silicon synthesized at room or lower temperatures which are typically not epitaxial.

However, the tabulated elemental sensitivity coefficients for bulk specimens cannot be used for subnanometer thick coating characterization. This latter application requires allowance for substrate contribution and atomic density which differ from those for the bulk. This allowance can only be made on the basis of experimental data obtained for other additional parameters or with an alternative analytical method. The simultaneous use of AES and EELS simplifies the task.

Furthermore, complex analysis with the two methods for the same probing depth of the structural, chemical and phase state of two-dimensional coatings and their interfaces with substrates provides additional possibilities [4,23], e.g.

- the dependence of the EELS peak energy and intensity on the primary beam energy provides information on the total thickness of the coating and, moreover, on the thickness of its layers and even on the interlayer spacing;
- the energy positions of the plasmon Auger peak satellites of the substrate atoms allows assessing the electron density in the coating directly at the substrate interface;
- quantitative Auger characterization with a simulated depth extinction function and characterization of two-dimensional coatings with nonuniform thickness;
- the dependence of the Auger peak intensity of the marker atoms on the substrate surface on the coating thickness can be used for localizing the positions of the adsorbed deposited atoms relative to the marker atoms.

In addition, AES provides understanding of coating growth mechanisms, i.e. layerwise, island, layerwise/island and more complex ones (e.g. mixing and/or segregation growth). EELS further allows tracking changes in the atomic density of coatings if they occur at unchanged element composition. Furthermore, one can detect changes in the state of the coating/substrate interface during the growth if AES and EELS are used simultaneously. This requires maintaining the same probing depth for the methods which should cover the growing film and reach the interface. Then, knowing the extinction function from the AES data and detracting the substrate contribution from the EELS spectra one can evaluate the electron density in the coating. And, vice versa, subtracting the coating contribution one can calculate the electron density in the substrate in the vicinity of the interface. One can also determine the coating growth mechanism and thickness based on solely the AES data for the same probing depth, by choosing between possible mechanisms. This requires applying the Auger analysis iteration, first for small coatings within the simplest growth model (typically, layerwise) and then for other coatings by verifying the growth mechanism at each iteration stage.

The first two-dimensional coatings were grown and studied on silicon [17] as this material is the most widely used substrate in the microelectronics technology. We also grew and characterized these coatings with AES and EELS. The targets of the study were the interface formation processes and the transient *3d* metal (Cr, Co, Fe, Cu) / silicon system.

This system exhibits strong interaction between the metal and the substrate, this being the cause of two-dimensional coating formation at greater than monolayer thicknesses. As has become clear by now, these coatings have a nanophase structure and exhibit wetting thermodynamic properties [4]. We obtained wetting layers of silicides and metals on silicon. This was achieved by reducing the heat power of the vapor source and modifying the source design by sputtering the evaporated material on a tantalum ribbon [24]. As a result we could study two VPD modes [4]:

- high-temperature (conventional) growth causing interdiffusion between the metal and the silicon substrate;
- low-temperature (lowered beam temperature) growth providing for an almost pure metal coating.

There are no literary data on this simultaneous used of AES and EELS, and we therefore will mainly dwell upon the unique experimental results.

This work is a compilation of experimental results on the variety of AES and EELS capabilities in the study of the structural phase and chemical state of two-dimensional coatings and their interfaces during the growth. Our emphasis was on the early growth stages in the transient *3d* metal (Cr, Co, Fe, Cu) / silicon system.

AES composition and growth mechanism analysis of two-dimensional coatings

Quantitative Auger characterization of binary coatings

Auger analysis of nonuniform thickness nanostructures consisting of a binary two-dimensional coating $A_xB_{(1-x)}$ and a substrate $A_yB_{(1-y)}$ is of special importance for the study of the early growth stages of these nanostructures. Examples are two-dimensional silicide phases on silicon forming at an early silicide growth stage [4].

The thickness of the two-dimensional phases is typically smaller than the Auger electron depth and far smaller compared with the backscattered electron range. Therefore the two-dimensional phase contribution to the backscattering factor can be ignored for simplifying Auger analysis. For a quantitative characterization of a two-dimensional coating / substrate $A_xB_{(1-x)}$/ $A_yB_{(1-y)}$ structure in a binary intermetallic system *AB* one should determine three parameters: coating thickness, coating composition and substrate composition. As a rule, only one of these parameters is known, so the task is to find the other two. This can be done by measuring the peak intensities in the AES spectra (I*A* and I*B*) for two probing depths (D_s and D_v, where $D_s \ll D_v$). These probing depths are controlled by the AES peak energy (E_s and E_v) and the primary electron energy (E_0). If the coating thickness *d* and the

probing depth D satisfy the relationships $D_v \gg d$ and $D_s \sim d$, the following set of equations is true [23]:

$$\frac{I_A^s}{I_B^s} = \beta^s \frac{x[1 - F_A^s(d)] + yF_A^s(d)}{(1-x)[1 - F_B^s(d)] + (1-y)F_B^s(d)}; \quad (1)$$

$$\frac{I_A^v}{I_B^v} = \beta^v \frac{x[1 - F_A^v(d)] + yF_A^v(d)}{(1-x)[1 - F_B^v(d)] + (1-y)F_B^v(d)}; \quad (2)$$

$$\beta^{s(v)} = \frac{(1-z)I_{ZA}^{s(v)}}{zI_{ZB}^{s(v)}}, \quad (3)$$

where x, y, z are the concentrations of A in the surface coating $A_xB_{(1-x)}$, in the substrate $A_yB_{(1-y)}$ and in the reference specimen $A_zB_{(1-z)}$, respectively, F is the depth extinction function ($F = \exp(-d/D)$) for uniform media and depends on the depth D of the layers, the s and v indices refer to Auger electrons with low (30–150 eV) and high (500–2000 eV) energies, respectively, at which the probing depth with allowance for the free path length [10] and the shape of the cylindrical Auger reflection analyzer (the entrance angle is 0 arc deg and the exit angle is 45 arc deg) is in the ranges 0.25 nm for D_s and 0.5–9 nm for D_v, respectively.

Example of quantitative Auger characterization of Cr on Si and Si on $CrSi_2$ coatings was provided earlier in a tabulated form [23]. The matrix factor β was experimentally obtained for a homogeneous reference $A_zB_{(1-z)}$ specimen of the $CrSi_2$ composition.

These data along with the EELS peak depth profiling [23] can be used for the structural modeling of the two-dimensional phases. One should, however, bear in mind that Eqs. (1)–(3) are only true in the abovementioned assumptions.

Quantitative Auger Characterization of Two-Dimensional Coatings (borrowed from [23]).

Type of Two-Dimensional Coatings	Substrate Composition A_yB_{1-y}, molar fractions	Coating Composition A_xB_{1-x}, molar fractions	Coating Thickness, mn	Chemical Formula
Si(111)-1 × 1-Cr (s-alloy)	0	0.10	0.39	$CrSi_9$
Si(111)-α($\sqrt{3} \times \sqrt{3}$)R30°-Cr	0	0.28	0.33	$CrSi_3$
Si(111)-β($\sqrt{3} \times \sqrt{3}$)R30°-Cr	0	0.40	0.71	Cr_2Si_3
$CrSi_2$(0001)-1 × 1-Si	0.33	0.03	0.125	Si

Auger analysis by substrate marker atom signal extinction

Surface atoms S in a submicron thickness two-dimensional coating may have the following positions relative to the marker atoms M on the substrate surface:

- type A: S over M;
- type B: S between M;
- type C: S over and between M.

Obviously, the signal extinction of the substrate atoms M will differ depending on their positions: strong for the type A, weaker for the type B and moderate for the type C. The degree of Auger peak extinction for the marker atoms M can be determined from the atom arrangement type (adsorption type) in the surface coating S, i.e., A, B or C. moreover, one can observe a change in the adsorption type, e.g. A to C transition.

The pattern of Auger peak extinction for the marker atoms (M are Cr atoms) for Si growth on (0001) $CrSi_2$ at the minimum primary beam energy (300 eV) well illustrates this latter possibility [23] (Fig. 1). As can be seen from Fig. 1, for a 0.2 nm/min Si deposition rate and a 0 to 1/3 Si monolayer (ML) thickness (0–0.117 nm) the M (Cr) Auger peak extinction is anomalously strong and the S (Si) adsorption is A type one. However, in the 1/3 to 1 ML Si monolayer thickness range (0.351 nm) the M peak extinction decelerates abruptly (B type adsorption) and a Si monolayer forms. Following this the M peak extinction is more moderate and obeys an exponential law, indicating C type adsorption with the pseudo-layerwise growth of a continuous Si coating.

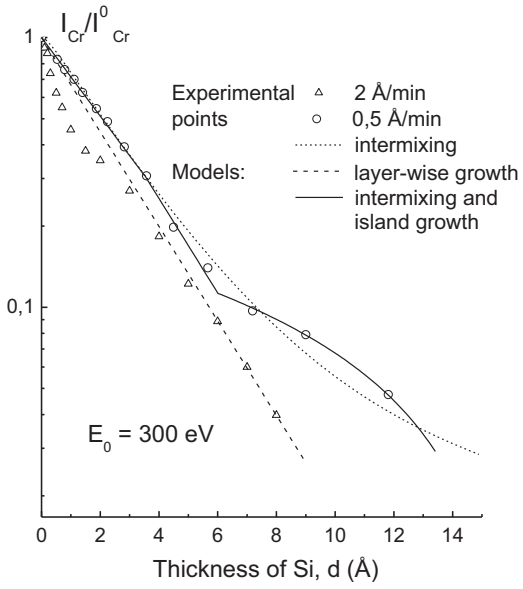

Fig. 1. Cr/(0001)$CrSi_2$ auger peak intensity ratio as a function of Si film thickness for Si deposition rates [23]: (△) 0.2 nm/min; (○) 0.05 nm/min.

At low Si deposition rates (0.05 bn/min) the Si atoms initially mix with the substrate (B type adsorption), followed by C type adsorption a pseudo-layer type growth of a nonequilibrium wetting Cr_xSi_{1-x} layer up to 0.6 nm in thickness. Bulk Si islands form at the final process stage.

The growth models based on the assumption of an exponential extinction function F and on simplified expressions similar to Eqs. (1)–(3) describe the above described adsorption types for different growth stages adequately well [23].

Quantitative Auger analysis of coating growth mechanisms

Theoretical simulation of experimental curves allows quantitative description of coating growth (the composition and thickness of the growing layers) provided that the growth mechanism is known or derived from the simulation of experimental curves.

A specific feature of the transition metal coating / silicon substrate system is the formation of wetting two-dimensional (2D) layers of a metal or its melt with silicon at an early growth stage and island growth after the transition of the wetting layer to a bulk (3D) phase. Thus, the system exhibits either pseudo-layerwise growth for which the layer continuity is not violated during the 2D–3D transition, or layerwise/island growth.

Fig. 2 shows Auger peak intensity vs layer thickness for Fe coatings on (001) Si 2 × 1 arrangement at (a) low and (b) high Fe beam temperature [4]. The substrate Auger peak deviation from the theoretical layerwise growth curve (dashed curve) provides information on the growth mechanism. Based on the data on possible growth mechanisms in the system (see above) one can simulate these growth mechanisms and choose the best fitting one.

The solid curves in Fig. 2 show the curves for the chosen growth models at different growth stages (I, II, III).

1. Stage I is the formation of a Fe–Si solid solution caused by the diffusion of ~1.5 ML Si from the substrate (Fig. 2a) or FeSi silicide (Fig. 2b).

2. Stage II is the growth of the Fe coating with the segregation of 0.45 ML Si layer (Fig. 2a) or Fe_3Si silicide formed by mixing of Fe with 3 ML Si (Fig. 2b).

3. Stage III is the layerwise Fe growth (Fig. 2b).

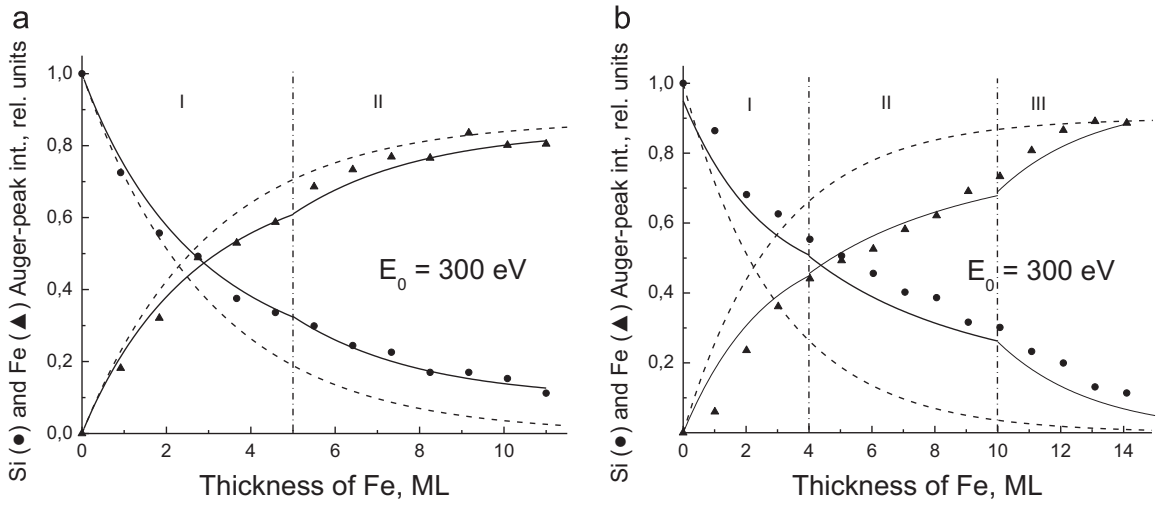

Fig. 2. Si and Fe auger peak intensities as a function of Fe film thickness on (001) 2×1 Si for two Fe source temperatures [4]: (*a*) low (1240 °C); (*b*) normal/high (1400 °C).

Iteration Auger analysis of coating thickness and growth mechanism

The iteration procedure contains several sequential approximations of the coating thickness with an increase in the number of the initial points of the Auger curve used for the assessment, and with growth mechanism model correction (Fig. 3) [4].

The zero approximation of the coating thickness (Y axis scale in Fig. 3) was made based on the data on the first deposited Fe layer (for submonolayer coatings) in the assumption of a pseudo-layerwise growth mechanism (curve *1*). The Auger peak extinction function was approximated by the F function (see above) for λ ~ 3 ML probing depth.

The next depth approximation was based on the several first layers (points) in a more realistic growth mechanism assumption which followed from curve analysis. Then the next growth model was accepted (curves *2–5*). Further approximation and growth models can be made until the final thickness estimate and growth mechanism model are accepted.

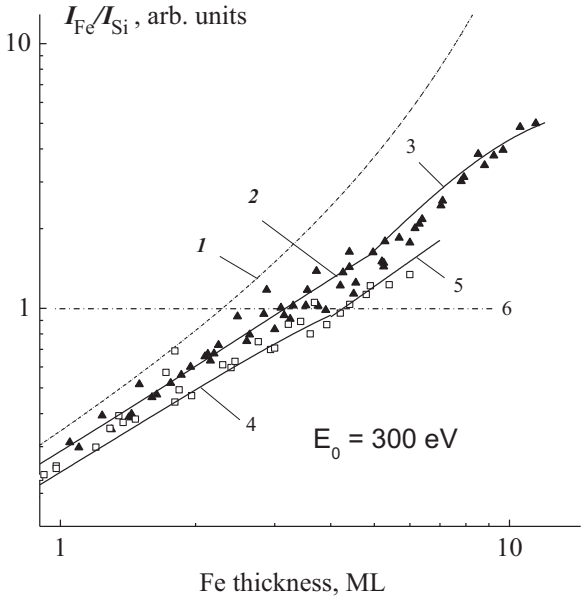

Fig. 3. Fe on (001) Si coating thickness and growth mechanism approximation by iteration for two deposition modes: (*2*, *3* and ▲) low temperature and (*4*, *5* and □) normal [4]. (*1*) layerwise (pasudo-layerwise) growth.

Simultaneous AES and EELS phase structure analysis

The simultaneous use of AES and EELS with the same probing depth allows differentiating the phases by composition and atomic density provided their composition is similar. Similar phase composition means the same number of electrons in the valence bonds. The plasmon loss peak position in the EELS spectra determines the concentration of valence electrons per unit volume. Therefore the position of this peak allows assessing the bulk atomic density of a phase for a constant composition. If the composition changes gradually during the growth as confirmed by the AES data, a change in the bulk atomic density during phase transitions causes a stepwise change of the peak position in the EELS spectrum.

Moreover, knowing the coating thickness from the AES data one can make allowance for the substrate EELS signal extinction due to signal passage through the coating and thus subtract the substrate contribution from the total EELS spectrum [4]. As a result one can have a more detailed vision of the EELS spectrum of the coating and changes in the EELS spectrum of the substrate/coating interface layer if any.

For constant phase composition or density during coating synthesis, the EELS spectrum correlates with composition changes. For example, one can observe the formation of a multilayered coating from phases of different *3d* metals. Otherwise there is a correlation with changes in the atomic density if the coating composition changes gradually (e.g. for gradual mixing between the coating and the substrate) or remains constant (growth of pure metal or silicon on silicide). Changes in atomic density are most expressed in the EELS spectra after the formation of a 2D wetting layer, i.e. its transition to a bulk phase, because the atomic density of the wetting layer is much different from the bulk atomic density.

Of special importance for the AES/EELS structural phase analysis is the probing depth. We found that for the simultaneous AES and EELS analysis of subnanometer thick coatings (1–10 ML) and their substrate interfaces the optimum probing depth is 3 ML. This probing depth is achieved at a primary electron energy of ~300 eV, both for AES and EELS [4,23,24].

EELS analysis of phase transitions

The composition of a forming interface (Figs. 1–3) changes gradually. This allows EELS analysis of phase transitions which can be compared with the AES data on the growth stages.

Fig. 4 shows families of EELS spectra illustrating the changes at the same Fe / (001) Si substrate interface as in Fig. 2 for different growth modes, i.e. normal and low-temperature [4]. It can be seen from Fig. 4

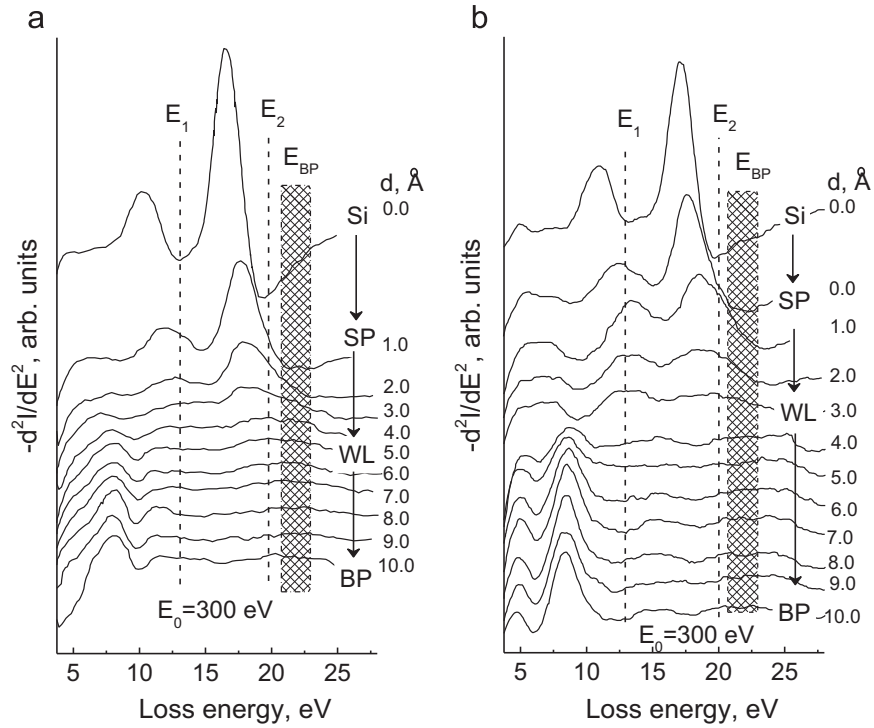

Fig. 4. EELS spectra of Fe coating on (001) Si during interface formation for two growth modes:.
(*a*) mixing (high temperature mode) and (*b*) no mixing (low temperature mode) between Fe film and Si substrate. E_1 and E_2 coating surface and bulk plasmon loss peak positions, respectively; EBP is the bulk phase (metal and silicide) bulk plasmon loss peak, SP, WL and BP are surface phase, wetting layer and bulk phase, respectively.

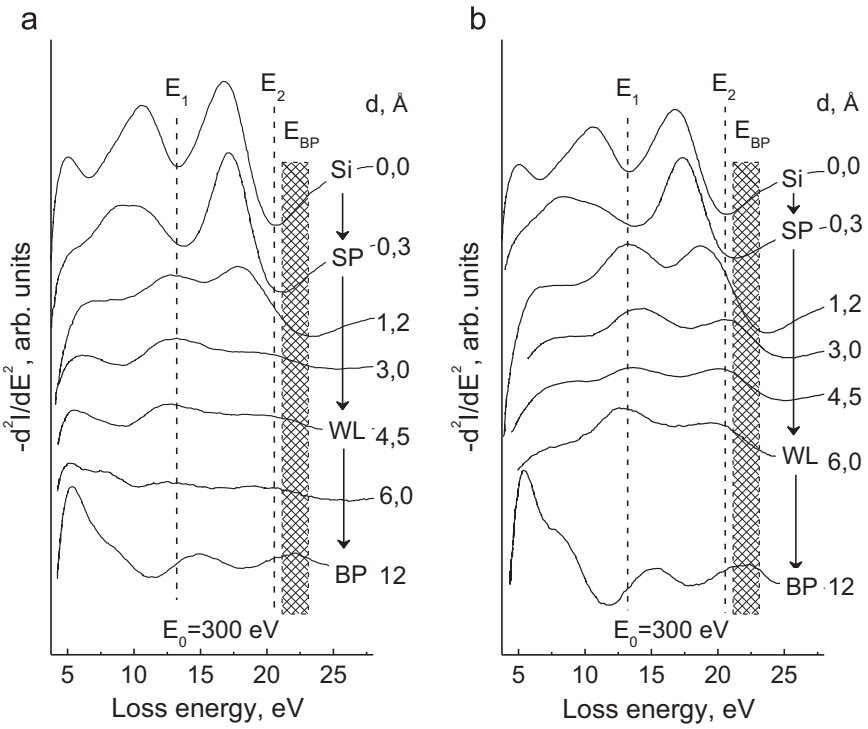

Fig. 5. Fe on (001) Si coating EELS spectra for different thicknesses [4]: (*a*) as-deposited; (*b*) as-annealed (250 °C).

that an increase in the coating thickness causes the intensities of some surface and bulk plasmon loss peaks to increase or decrease. The substrate peaks intensities deplete to zero, and eventually a bulk phase peak develops. However, this latter peak grows with a delay for relatively thick coatings (typically at least 3 ML).

This delay is also caused by the formation of a 2D wetting layer having the composition (a) FeSi or (b) Fe + ~1.5 ML Si. This layer does not have any expressed plasmon loss peaks because of its nanophase (fine-grained and inonuniform density) structure. The same behavior is observed for the EELS spectra during the formation of other interfaces, i.e. Cr/Si(111), Fe/Si(111), Co/Si(111) and Cu/Si(001) [4,23–27].

Thus, the formation of a wetting metal layer on silicon under nonequilibrium conditions (deposition at room temperature) is a general regularity of metal/silicon interface formation. The wetting layer was not observed earlier because the interface formation was not studied with both AES and EELS in an as detailed and integrated manner as in this work.

Meanwhile, the formation of a wetting layer is a multistage process preceded by the formation of various two-dimensional phases with different atomic densities and compositions.

Fig. 5 illustrates the evolution of the Fe / (001) Si interface during the transition from the as-deposited state (Fig. 5a) to the as-annealed at

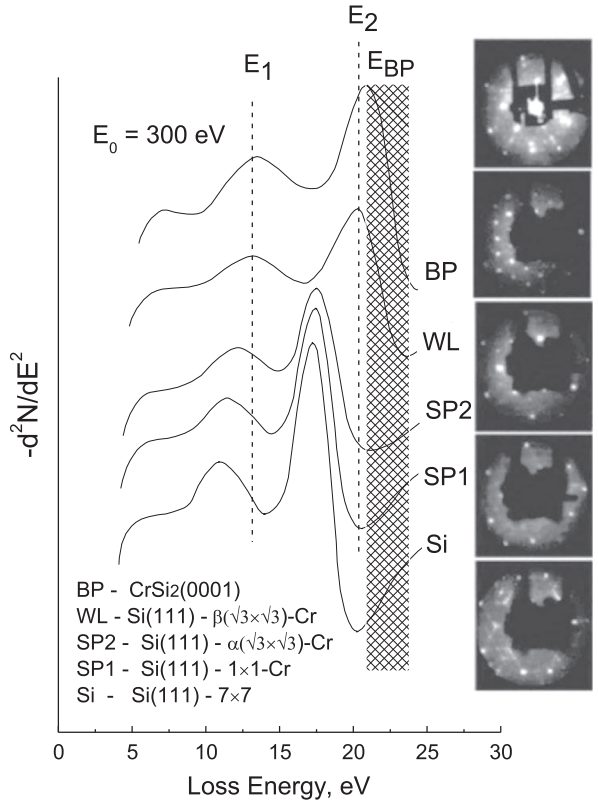

Fig. 6. EELS spectra and slow electron diffraction patterns [25] of Cr–Si coatings on (111) Si. At the right: Si substrate, SP are surface phases with a $(\sqrt{3}\times\sqrt{3})$ Structure, WL is the wetting layer with a $(\sqrt{3}\times\sqrt{3})$ structure, BP is the bulk phase / epitaxial silicide $CrSi_2$; E_1 and E_2 are the surface and bulk Loss peak energies in WL, respectively, and E_B is the bulk loss peak energy in the bulk phases of the Cr–Si system.

250 °C state (Fig. 5b). Same as discussed above, the bulk phase formation is delayed (in our case, bulk Fe) due to the formation of a nanophase wetting layer. However, annealing makes the wetting layer density more uniform and, probably, leads to a more ordered (epitaxial) layer structure. This is indicated by an increase in the plasmon loss peak intensity seen in Fig. 5b compared to that in Fig. 5a.

Higher annealing temperatures (> 350 °C) produce more ordered 2D phases (SP_1 и SP_2) and cause wetting layer (WL) and bulk silicide (BP) epitaxy (Fig. 6). All the phases have specific plasmon loss peak positions. These peaks are closer to the silicon peaks in the surface phases and to the bulk silicide peaks in the wetting layer.

Thus, AES and EELS phase structure analysis proves to be important for studying the formation of heterogeneous interfaces, allowing a more detailed tracing of interface formation stages under different deposition conditions.

Furthermore, AES and EELS phase structure analysis allows detecting atomic density changes which is of great importance for determining the conditions and mechanism of wetting layer formation and its transition to the first bulk phase. It also allows tracing the transition from an unordered (amorphous) state to an ordered (epitaxial) one.

EELS phase analysis with substrate contribution subtraction

I noted above that wetting layer formation is a multistage process. A more detailed vision of this process and the transition to a bulk phase can be attained by subtracting the substrate contribution to the EELS spectrum.

Precision evaluation of the substrate contribution is impossible because other contributions (those of the film and the interface layer) may change. One can however detract the substrate contribution using weight coefficients based on the in-depth film AES data or by fitting these coefficients to retain the shape of the bulk plasmon loss peak in the as-subtracted spectrum. One can then visualize finer changes in the spectra and understand which changes occurred in the interface layer and the film compared with the simple model for the bulk film phase / substrate without interface layer modification.

Fig. 7 shows EELS spectra for Cu coatings on (001) Si (a) before and (b) after substrate EELS contribution subtraction [27]. Fig. 8 shows EELS spectra for (a) Co coatings on (111) Si and (b) Fe coatings on (001) Si after substrate EELS contribution subtraction [4].

For the Cu coatings (Fig. 7) the subtraction shows that the bulk plasmon energy loss in the Cu layer is close to the plasmon energy loss in the bulk Cu or copper silicide phases (17.5 eV) already at a 1 ML thickness. The subtraction shows well the shift of the surface plasmon loss peak between the 5^{th} and 6^{th} monolayers for the bulk Cu. The screening length is ~1 ML in copper and ~2 binary layers in Si. Our assumption is that the bulk plasmon loss peak position is affected by the interface silicon layer (at a up to 1 monolayer stage) while the surface plasmon loss peak position (due to the coupling of the plasmon with the interface pl;plasmon) is affected by the interface film layer (at a 1–5 monolayers stage).

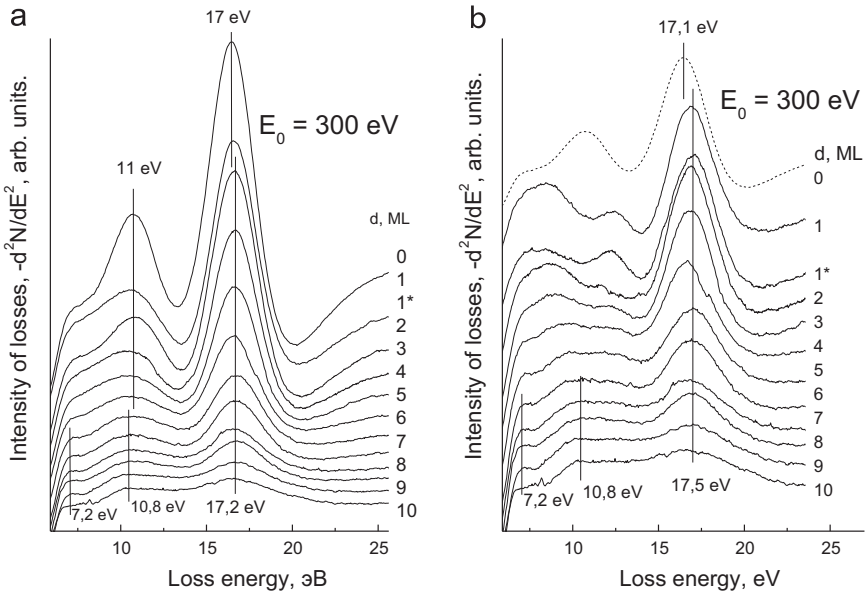

Fig. 7. EELS spectra (*a*) without and (*b*) with substrate contribution subtraction for (001) Cu/Si [27].

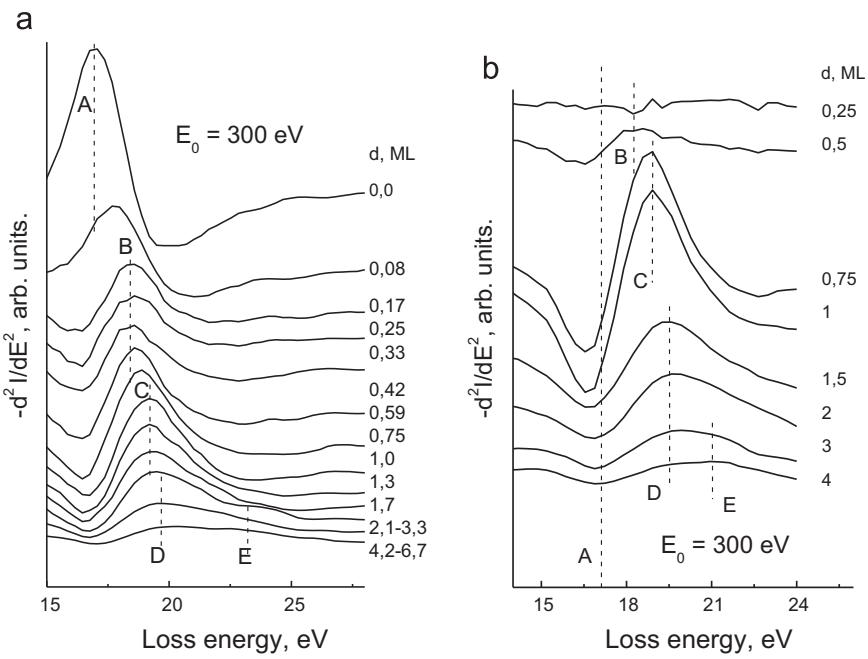

Fig. 8. EELS spectra with substrate contribution subtraction for (*a*) (111) Co/Si [26] and (*b*) (111) Fe/Si [4].

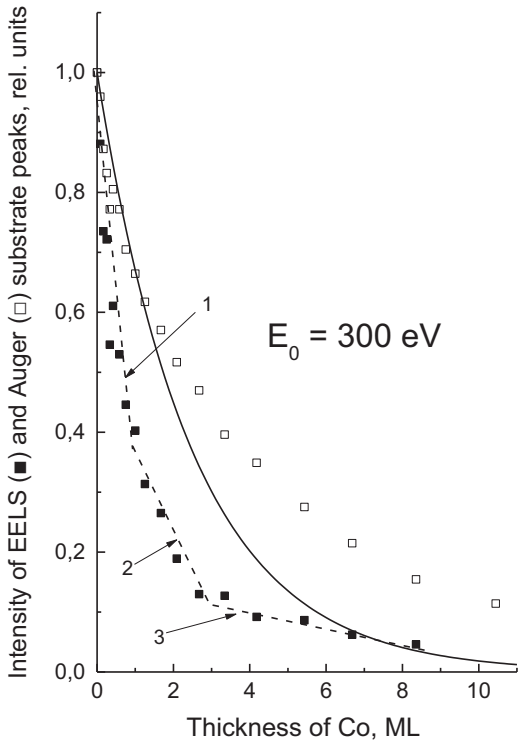

Fig. 9. Intensity ratio of (■)Si bulk plasmon Loss peak in the EELS spectrum and (□) Si auger peak for Co on (111) Si as a function of thickness [26]. Solid line is the theoretical function for pseudo-layerwise growth (exponential extinction); dashed line shows plasmon loss peak extinction stages (*1*, *2*, *3*).

For the Co and Fe coatings (Fig. 8), the subtraction allows separating intermediate surface phases (peak *B*) forming during the formation of the wetting layer and assessing the thickness range of their formation. These phases form in subnanolayer coatings and in single monolayer coatings (peak *C*), along with the wetting layer (peak *D*), typically in the 2 to 3 monolayer range. The allowance for the phase layer thickness as well as the phase composition, electron density and growth mechanism provides understanding of the respective phase growth models. For example, the average electron density in the wetting layer and the scatter of this density as indicated by the shape of the bulk plasmon loss peak can be accounted for by a nanophase structure of the wetting layer. This structure is typical of a set of close-packed and elastically strained nanoclusters.

Fig. 9 shows the relative intensity of the bulk plasmon loss peak in the EELS spectrum of the Co coatings on (111) Si for different thicknesses [26]. The theoretical curve for pseudo-layerwise growth is the same for substrate Auger peak extinction (without mixing) and substrate loss peak (with a constant plasma concentration in the interface layers). Furthermore, Fig. 9 shows the experimental substrate Auger peak extinction and dashed curves for different plasmon loss peak extinction stages (1, 2 and 3).

The deviation of the experimental points for the Auger peak from the theoretical curve for Co layer thicknesses of greater than 1–1.5 monolayers indicates that after this thickness is reached the Co atoms mixed with Si atoms of the substrate. However, mixing does not occur if the thickness is within 1 monolayer (stage 1), but the loss peak extinct much faster than for the perfect model (solid line). Thus, the valence electron plasma region for which the concentration differs from that of the substrate broadened toward the substrate. This indicates that the interface layer with a different valence electron concentration forms in silicon. This can be caused by a chemical interaction between the Si interface layer with Co. As a result a two-dimensional covalence bond region forms between Si and Co (within the Debye screening length), accompanied by the formation of an elastic nanostructure in the interface layer. Indeed, the subtraction of the substrate spectrum (Fig. 8a) revealed the formation of surface phases at that stage, with the concentration of the valence electrons in these phases being close to that for silicon but higher.

Stage 2 (1–3 M, Fig. 9) is manifested by the formation (growth) of a Co wetting layer. The parallel course of the experimental and theoretical extinction curves for this stage indicates that no fundamental changes occurred at the interface during the growth of the wetting layer. Thus, both the covalence film/substrate bond region and the elastically strained substrate interface region are retained.

At stage 3 (> 3 ML) the loss intensity extincts in a similar linear manner but far less slower. This can be caused by the lateral growth of the Co bulk phase islands and the depletion of the intermediate layer (the covalence film/substrate bond region and the elastically strained substrate region) resulting from the wetting layer – bulk phase transition.

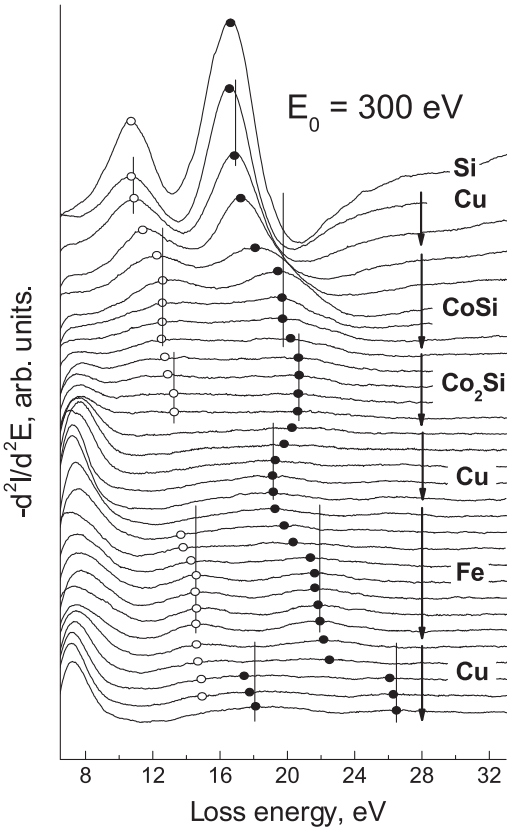

Fig. 10. EELS spectra of multilayered coatings Cu (8 ML) / Fe (8 ML) / Cu (5 ML) / Co (10 ML) / Cu (2 ML) on (001) Si at different growth stages [28]: ○, ■: surface and bulk plasmon loss peak positions, respectively.

Thus, analysis of the substrate plasmon peak extinction curve provides information on changes in its interface layer and the mechanism of the film/ substrate interaction. It is furthermore shown that simple subtraction of the substrate contribution without interface layer allowance is incorrect.

EELS analysis of multilayered coating growth stages

As noted above, if coatings consist of bulk phases the EELS spectrum correlates with the coating composition change. Figs. 10 and 11 show EELS spectra and Auger peak intensities for Cu (8 ML) / Fe (8 ML) / Cu (5 ML) / Co (10 ML) / Cu (2 ML) multilayered coatings on (001) Si during their growth [28].

The EELS spectra and the surface and bulk plasmon loss peak positions in Fig. 10 show the nanolayer growth stages. The growth of Cu, Co and Fe nanolayers exhibits a early stage of the wetting layer (with an undistorted bulk plasmon loss peak) and the further bulk layer growth stage (with the finally established bulk plasmon loss peak). Noteworthy, only the undistorted bulk plasmon loss peak is observed during the formation of the first (2 ML thickness, Cu_2Si composition as per the AES data, Fig. 11) and the intermediate (5 ML thick) two-dimensional Cu layers (AES data, Fig. 11). In the meantime, the formation of the intermediate Co layer is accompanied by a sequential formation of CoSi and Co_2Si silicides (Fig. 11) caused by intense interdiffusion with the substrate (the first three layers were deposited at 250 °C [28]).

These changes would be clearer in higher resolution EELS spectra or after subtraction of the previous layer contributions. For example, it would be possible to define more clearly the growth stages by subtracting the previous spectrum from the subsequent one and introducing the weight coefficient to be proportional to the change of the relative substrate contribution to the spectrum (determined from the AES data and the growth model).

Interface phase analysis from AES Data

Typically, the Auger spectra contain satellite peaks resulting only from the energy structure of the valance band. However, analysis of the satellite plasmon loss peak position in the Auger spectra provides additional advantages.

Figs. 12 and 13 show Auger data on the fine structure of the $L_{23}VV$-Si peak during the growth of Cr [24] and Fe [4], respectively. The peak fine structure contains the main $L_{23}VV$-Si peak and the plasmon satellite peak formed by the plasma oscillation Auger electron $L_{23}VV$ losses in the neighborhood of silicon atoms. Since silicon is either in te substrate or in the coating, this satellite illustrates the silicon neighborhood in te substrate and in the coating. Thus, it allows differentiating whether there is mixing between silicon and the metal and tracking density changes in the vicinity of the silicon atoms.

It can be seen from Fig. 12 that the pure Cr peak grows with an increase in the coating thickness (especially at the 7×7-Cr phase, Fig. 12 *b*) because after the thickness reaches 4 monolayers the plasmon satellite energy becomes equal to that of pure Cr. Taking into account the probing depth (~3 ML) this early peak development is possible provided there is no mixing. However, at 2–3 ML thicknesses a Cr wetting layer forms because the bulk Cr peak is not yet developed. Obviously, the peak development stages can be separated by subtracting the substrate contribution from the spectra shown in Fig. 12b. this naturally requires a higher spectral resolution.

Fig. 13 shows Auger peaks of the Fe coatings on (001) Si grown at low and high metal flux temperatures. Analysis of the Fe to Si peak amplitude ratio in Fig. 13 showed that in the former case (low temperature growth) the Fe peak grows without mixing while in the latter case (high temperature growth) the Fe peak growth is accompanied by mixing with Si resulting in the formation of FeSi and Fe_3Si. The plasmon satellite position in the former case shows the formation of the Fe wetting layer and in the latter case the Fe–Si wetting layer. Then these layers transform to bulk Fe and silicide FeSi phases. The peak in the 67–75 eV range is related to the bulk plasmon loss $L_{23}VV$ of Auger electrons at approx. 92 eV. An increase in its energy indicates the formation of a denser bulk Fe phase (Fig. 13a) or denser silicides (Fig. 13b). The disappearance of that peak in Fig. 13a after 5 ML thickness can be caused by the formation of a cluster or fine-grained structure in the Fe coating. Such structures have nonuniform electron density under these conditions and therefore their peak is smeared and has low amplitude. However, the plasmon satellite position in Fig. 13b at ~5–14 ML thicknesses corresponds to the FeSi to Fe transition the bulk plasmon energies of which are 21 and 25 eV, respectively [29,30].

The increase in the energy of the satellite peak in the 77–80 eV range attributed to the bulk *sp* states of Si is caused by an increase in the number of Fe atoms in the Si neighborhood. The shift of that peak in

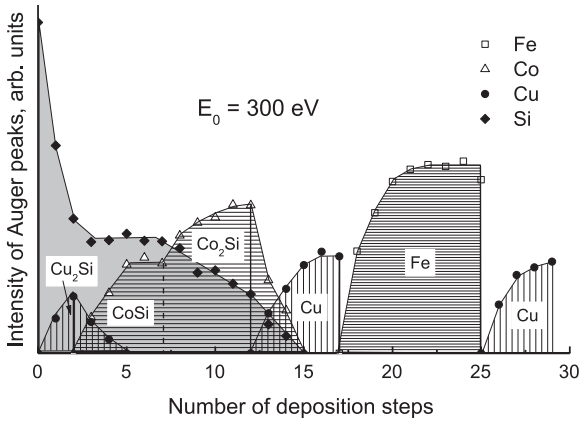

Fig. 11. Auger peak intensitites in the AES spectra and layer compositions at different growth stages of multilayered coatings Cu (8 ML) / Fe (8 ML) / Cu (5 ML) / Co (10 ML) / Cu (2 ML) on (001) Si [28].

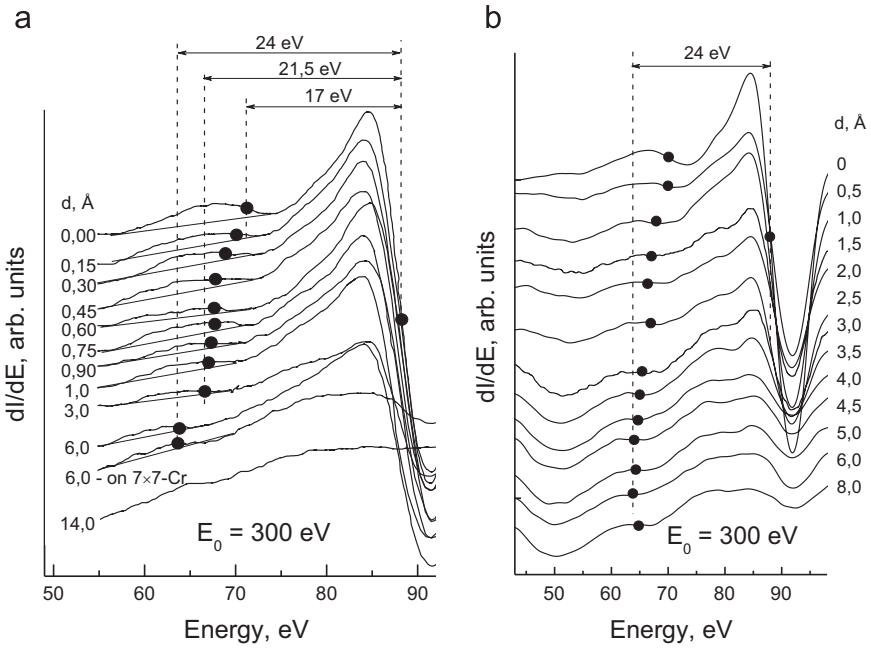

Fig. 12. Plasmon satellite in AES spectra of (*a*) Cr coatings on (111) Si [24] and (*b*) with coatings on the 7 × 7 Cr surface phase.

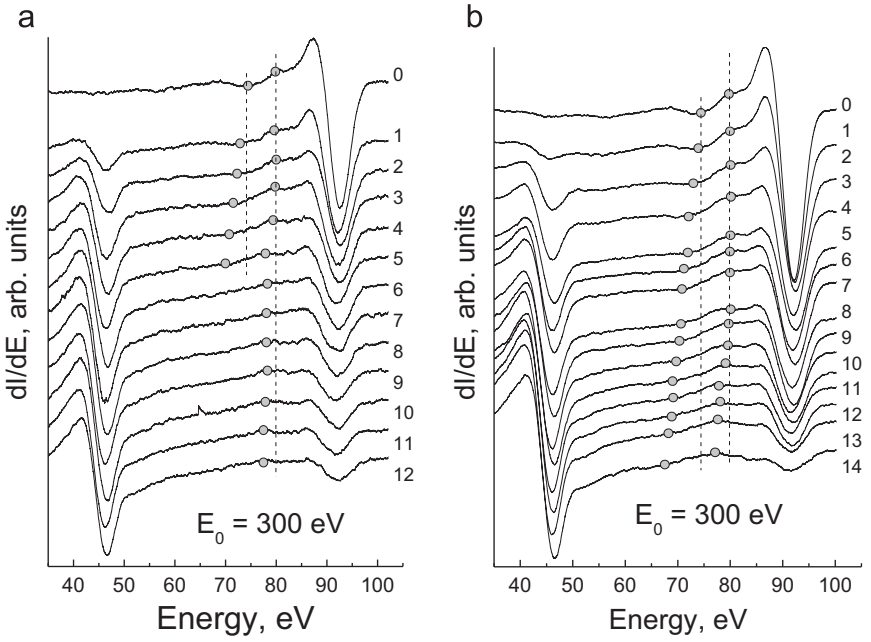

Fig. 13. Plasmon satellite in AES spectra of Fe on (001) Si [4]: (*a*) growth without mixing; (b) growth with mixing.

Fig. 13a suggests that after 5 ML thickness the Si atoms have the same neighborhood as in the bulk Fe phase. The retention of that peak at 12 ML shows that the surface of the bulk Fe phase has a segregated ultrathin Si layer (~ 0.5 ML according to the AES data). In the meantime, the position of that peak in Fig. 13b corresponds to the formation of FeSi at an early stage (after 5–6 monolayers) and then to the formation of Fe_3Si (after 10 monolayers). Thus, for a 5 monolayer thick coating a Fe and iron silicide wetting layer forms in both cases.

The behavior of the silicon plasmon satellite peak was studied as a function of Co film thickness on a (111) 7 × 7 Si substrate (Fig. 14). The experimental data illustrated in Fig. 14 suggest the following growth stages:

I. formation of a surface phase at 0.2–0.5 ML coating thickness;
II. formation of a Co monolayer at 0.5–1 ML coating thickness;
III. final stage of Co wetting layer formation at 2–3 ML coating thickness.

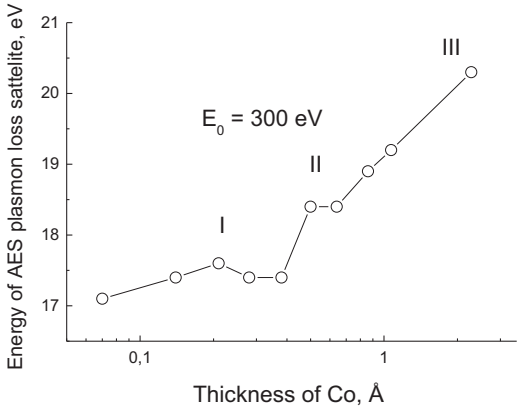

Fig. 14. AES spectrum plasmon satellite $L_{23}VV$ energy as a function of thickness and three growth stages (I–III) of Co coating on (111) 7 × 7 Si (data borrowed from [26]).

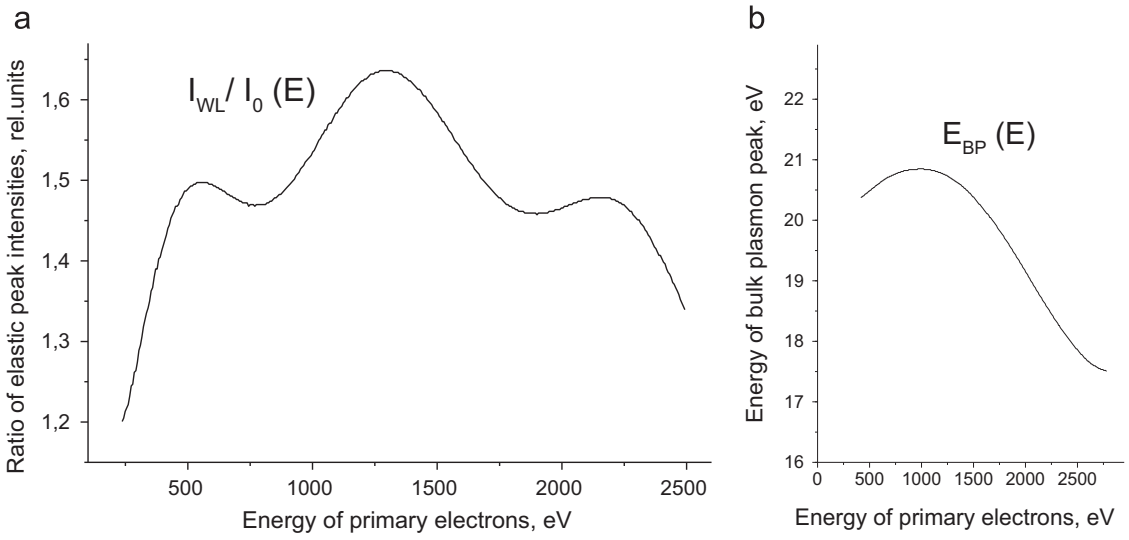

Fig. 15. (*a*) Ratio between the elastic peak intensity of ordered Cr–Si wetting layer with a $\sqrt{3} \times \sqrt{3}$ (I_{WL}) structure and the respective peak intensity I_0 for surface rearrangement of (111) 1 × 1 Si substrate with Cr coating as a function of probing depth and (*b*) bulk plasmon loss energy in the silicide layer as a function of primary electron energy [23].

EELS depth profiling

While EELS analysis does not find general application today, analysis of energy functions EELS(E) is even less used. This is quite a labor consuming method requiring thorough methodical development, improved tools and measurement automation. Evidently, though, these energy functions characterize the diffraction at the lattice planes of the superficial region, which provides information on the interplane spacing, and the backscattering factor distribution, which characterizes the atomic composition depth profiles.

As can be seen from Fig. 15, the relative intensity of the elastic peak function $I_{WL}/I_0(E)$ and the plasmon oscillation bulk loss energy function $E_{BP}(E)$ in fact provide the atomic composition depth profiles of surface regions and allow measuring atomic layer depths in the wetting layer WL and the thickness of the silicide layer.

The resultant composition profiles allow modeling the WL layer which has a thickness of ~12 ML, or about two double layers of the (111) Si lattice, and contains three Cr layers: one on the surface and two interstitial intercalated layers.

Summary

Two additional capabilities of the AES and EELS methods were shown for the characterization of two-dimensional coatings and their interfaces. These capabilities were demonstrated with a study of early growth stages of monolayer and multilayere metallic coatings on silicon and their physical vapor deposition modes.

Compared with the conventional AES and EELS analysis the new method allows correct comparison between AES data on the composition and electron energy structure and EELS data on the spatial structure of valence electrons. The use of the same probing depth for AES and EELS allows identifying a wetting nanophase layer at its formation stage and its transition to a bulk phase, as well as the changes occurring at these stages near the substrate interface.

New capabilities were demonstrated for quantitative Auger analysis with two probing depths, analysis of plasmon satellite loss peaks in AES, study of EELS(E) dependence on primary electron energy, marker atom signal extinction pattern at the interface, EELS spectra with subtracted substrate or coating contribution, and iteration analysis of coating thickness and growth mechanism.

References

[1] G. Fiori, F. Bonaccorso, G. Iannaccone, T. Palacios, D. Neumaier, A. Seabaugh, S.K. Banerjee, L. Colombo, Electronics based on two-dimensional materials, Nat. Nanotechnol. 9 (2014) 768–779, http://dx.doi.org/10.1038/nnano.2014.207.
[2] D.V. Gruznev, A.V. Zotov, A.A. Saranin, One-atom-layer compounds on silicon and germanium, Jpn. J. Appl. Phys. 56 (8S1) (2017) 08LA01, http://dx.doi.org/10.7567/JJAP.56.08LA01.
[3] N.I. Plyusnin, Metallic nanofilms on single crystal silicon: growth, properties and applications, Izvestiya Vysshikh Uchebnykh Zavedenii. Materialy Elektronnoi Tekhniki = Mater. Electron. Eng. 18 (2) (2015) 81–94, http://dx.doi.org/10.17073/1609-3577-2015-2-81-94 In Russ..
[4] N.I. Plusnin, Atomic-scale AES-EELS analysis of structure-phase state and growth mechanism of layered nanostructures, Adv. Mater. Phys. Chem. 6 (7) (2016) 195–210, http://dx.doi.org/10.4236/ampc.2016.67020.
[5] Methods and phenomena: their applications in science and technology. Vol. 1: Methods of Surface Analysis, A. W. Czanderna (Ed.), Amsterdam; Oxford; New York; Tokyo: Elsevier, 1975. pp. 480. ⟨http://dx.doi.org/10.1016/B978-0-444-41344-4.50004-5⟩.
[6] H. Lüth, Solid Surfaces, Interfaces and Thin Films 4 Springer-Verlag, Berlin; Heidelberg, 2001, p. 589, http://dx.doi.org/10.1007/978-3-662-04352-3.
[7] Topics in current physics. Vol. 4: Electron Spectroscopy for Surface Analysis. H. Ibach. (Ed.), Berlin; New York: Springer-Verlag, 1977. pp. 255.
[8] L.J. Brillson, The structure and properties of metal-semiconductor interfaces, Surf. Sci. Rep. 2 (2) (1982) 123–326, http://dx.doi.org/10.1016/0167-5729(82)90001-2.
[9] P.W. Palmberg, Quantitative Auger electron spectroscopy using elemental sensitivity factors, J. Vac. Sci. Technol. 13 (1) (1976) 214–218, http://dx.doi.org/10.1116/1.568853.
[10] Practical surface analysis. Auger and x-ray photoelectron spectroscopy. D. Briggs, M. P. Seah (Eds.). Chichester; New York: John Wiley & Sons Ltd., 1983. pp. 548.
[11] R.E. Honig, Surface and thin film analysis of semiconductor materials, Thin Solid Films 31 (1–2) (1976) 89–122, http://dx.doi.org/10.1016/0040-6090(76)90356-4.
[12] D. Briggs, J.T. Grant, Surface Analysis by Auger and X-ray Photoelectron Spectroscopy, Chichester (UK): IM Publications and Surface Spectra Limited, 2003 [840 p].
[13] Transmission Electron Energy Loss Spectrometry in Materials Science and the EELS Atlas, Ed. by C. C. Ahn. Weinheim: Wiley-VCH, 2004. 457 p. ⟨http://dx.doi.org/10.1002/3527605495⟩.
[14] J.M. Howe, V.P. Oleshko, Application of valence electron energy-loss spectroscopy and plasmon energy mapping for determining material properties at the nanoscale, J. Electron Microsc. 53 (4) (2004) 339–351, http://dx.doi.org/10.1093/jmicro/dfh044.
[15] M. Menyhard, A. Konkol, G. Gergely, A. Barna, Development in Auger depth profiling technique, J. Electron Spectrosc. Relat. Phenom. 68 (C) (1994) 653–657, http://dx.doi.org/10.1016/0368-2048(94)80028-6.
[16] A.S. Parshin, G.A. Alexandrova, A.E. Dolbak, O.P. Pchelyakov, B.Z. Ol'shanetskiĭ, S.G. Ovchinnikov, S.A. Kushchenkov, Reflection electron-energy-loss spectroscopy of Fe_xSi_{1-x} thin films, Tech. Phys. Lett. 34 (5) (2008) 381–383, http://dx.doi.org/10.1134/S1063785008050064.
[17] V.G. Lifshits, A.A. Saranin, A.V. Zotov, Surface Phases on Silicon: Preparation, Structures, and Properties, Wiley, Chichester (UK), 1994 [462 p].
[18] R. Wiesendanger, Scanning Probe Microscopy and Spectroscopy: Methods and Applications, Cambridge University Press, 1994 [637 p].

[19] Ch Linsmeier, Auger electron spectroscopy, Vacuum 45 (6–7) (1994) 673–690, http://dx.doi.org/10.1016/0042-207X(94)90108-2.
[20] G. Moretti, X-Ray Photoelectron and Auger Electron Spectroscopy. Handbook of Heterogeneous Catalysis. Part 3. Characterization of Solid Catalysts. 3.2. Chemical Properties. 3.2.3. Valence States, Wiley-VCH Verlag, Weinheim, 2008, pp. 1029–1039, http://dx.doi.org/10.1002/9783527610044.hetcat0052.
[21] R.F. Egerton, Electron Energy-loss Spectroscopy in the Electron Microscope, Springer Science & Business Media, New York; Dordrecht; Heidelberg; London, 2011 [491 p].
[22] V.G. Lifshits, Yu. V. Lunyakov, EELS Spectra of Surface Phases on Silicon, Dal'nauka, Vladivostok, 2004 [314 p. (In Russ.)].
[23] N.I. Plusnin, Application of AES and EELS for surface/interface characterization, J. Electron Spectrosc. Relat. Phenom. 137–140 (2004) 161–164, http://dx.doi.org/10.1016/j.elspec.2004.02.091.
[24] N.I. Plusnin, A.P. Milenin, B.M. Iliyashenko, V.G. Lifshits, Elevated rate growth of nanolayers of Cr and CrSi2 on Si(111), Phys. Low.-Dimens. Struct. no. 9–10 (2002) 129–146.
[25] N.I. Plusnin, N.G. Galkin, V.G. Lifshits, S.A. Lobachev, Formation of interfaces and templates in the Si(111)-Cr system, Surf. Rev. Lett. 2 (4) (1995) 439–449, http://dx.doi.org/10.1142/S0218625X9500039X.
[26] N.I. Plusnin, V.M. Il'yashenko, S.A. Kitan, S.V. Krylov, Formation of Co ultrathin films on Si (111): growth mechanisms, electronic structure and transport, Appl. Surf. Sci. 253 (17) (2007) 7225–7229, http://dx.doi.org/10.1016/j.apsusc.2007.03.001.
[27] N.I. Plyusnin, V.M. Il'yashchenko, S.A. Kitan', N.A. Tarima, Structural and phase transformations during initial stages of copper condensation on Si(001), J. Surf. Investig. X-ray, Synchrotron Neutron Tech. 5 (4) (2011) 734–745, http://dx.doi.org/10.1134/S1027451011060140.
[28] N.I. Plyusnin, V.M. Il'yashchenko, P.A. Usachev, V.V. Pavlov, Growth, structural and magnetic properties of Fe, Co and Cu nanolayers on the Si substrate, Tech. Phys. 60 (10) (2015) 1501–1507, http://dx.doi.org/10.1134/S1063784215100266.
[29] X. Wallart, H.S. Zeng, J.P. Nys, G. Delmai, Electron spectroscopy study of the Fe/Si (111) interface formation and reactivity upon annealing, Appl. Surf. Sci. 56–58 (pt. 1) (1992) 427–433, http://dx.doi.org/10.1016/0169-4332(92)90265-Y.
[30] E. Colavita, M. De Crescenzi, L. Papagno, R. Scarmozzino, L.S. Caputi, RoseiR., Tosatti E. Single-particle and collective excitations in ferromagnetic iron from electron-energy-loss spectroscopy, Phys. Rev. B 25 (1982) 2490–2502, http://dx.doi.org/10.1103/PhysRevB.25.2490.